

PRODUCTION OF COLD ANTIHYDROGEN WITH ATHENA FOR FUNDAMENTAL STUDIES

A. KELLERBAUER¹, M. AMORETTI^{2,3}, C. AMSLER⁴, G. BONOMI¹, P. D. BOWE⁵, C. CANALI^{2,3},
C. CARRARO^{2,3}, C. L. CESAR⁶, M. CHARLTON⁵, M. DOSER¹, A. FONTANA^{7,8}, M. C. FUJIWARA⁹,
R. FUNAKOSHI¹⁰, P. GENOVA^{7,8}, J. S. HANGST¹¹, R. S. HAYANO¹⁰, I. JOHNSON⁴,
L. V. JØRGENSEN⁵, V. LAGOMARSINO^{2,3}, R. LANDUA¹, E. LODI RIZZINI^{12,8}, M. MACRÌ^{2,3},
N. MADSEN¹¹, G. MANUZIO^{2,3}, D. MITCHARD⁵, P. MONTAGNA^{7,8}, H. PRUYS⁴, C. REGENFUS⁴,
A. ROTONDI^{7,8}, G. TESTERA^{2,3}, A. VARIOLA^{2,3}, L. VENTURELLI^{12,8}, D. P. VAN DER WERF⁵,
Y. YAMAZAKI⁹, N. ZURLO^{12,8}

¹*Department of Physics, CERN, 1211 Genève 23, Switzerland*

²*Dipartimento di Fisica, Università di Genova, 16146 Genova, Italy*

³*INFN Sezione di Genova, 16146 Genova, Italy*

⁴*Physik-Institut, University of Zurich, 8057 Zürich, Switzerland*

⁵*Department of Physics, University of Wales Swansea, Swansea SA2 8PP, UK*

⁶*Instituto de Física, Universidade Federal do Rio de Janeiro, Rio de Janeiro 21945-970, Brazil*

⁷*Dipartimento di Fisica Nucleare e Teorica, Università di Pavia, 27100 Pavia, Italy*

⁸*INFN Sezione di Pavia, 27100 Pavia, Italy*

⁹*Atomic Physics Laboratory, RIKEN, Saitama 351-0198, Japan*

¹⁰*Department of Physics, University of Tokyo, Tokyo 113-0033, Japan*

¹¹*Department of Physics and Astronomy, University of Aarhus, 8000 Aarhus C, Denmark*

¹²*Dip. di Chimica e Fisica per l'Ingegneria e per i Materiali, Università di Brescia, 25123 Brescia, Italy*

(ATHENA Collaboration)



Since the beginning of operations of the CERN Antiproton Decelerator in July 2000, the successful deceleration, storage and manipulation of antiprotons has led to remarkable progress in the production of antimatter. The ATHENA Collaboration were the first to create and detect cold antihydrogen in 2002, and we can today produce large enough amounts of antiatoms to study their properties as well as the parameters that govern their production rate.

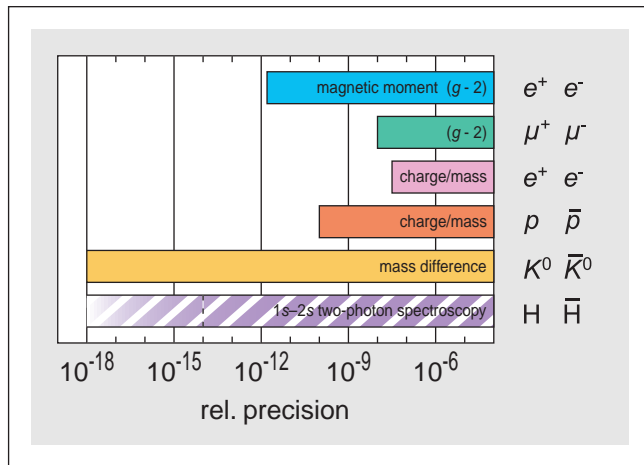


Figure 1: Comparison of experimental CPT tests for various classes of particle–antiparticle pairs with the *potential* for a CPT test with antihydrogen, based on the currently achieved precision in the determination of the hydrogen $1s$ – $2s$ transition frequency (10^{-14}) [9] and the limit due to its natural linewidth (10^{-18}).

1 Introduction

In 1957, the invariance of all laws of physics under the parity transformation (the reversal of the spatial configuration) was shown to be strongly violated in the weak decay [1]. The failure of such a fundamental symmetry, which was until then universally believed to hold, reminded scientists that human intuition can be treacherous in our quest to more fully describe nature. This realization, along with the discovery of the more subtle violation of CP symmetry (simultaneous reversal of charge and space) [2], has made physicists wary that the last of the fundamental symmetries, CPT, may also eventually be shown to be broken by sufficiently precise experiments. According to the CPT theorem, which also establishes an intimate link between CPT symmetry and Lorentz invariance, the simultaneous reversal of charge, space, and time transforms any particle into its antiparticle [3]. Particles and their antiparticles hence share many of their fundamental properties (such as mass and half-life), and some other properties are equal in magnitude and reversed in sign (such as charge and magnetic moment). Any difference of those properties between particle–antiparticle pairs would therefore be a clear proof of CPT violation and an indication of physics beyond the Standard Model. Spurred by the failure of C and CP and by recent theories that suggest the possibility of CPT violation [4, 5], experimental comparisons of particle–antiparticle pairs have been performed on all classes of particles and to quite high precision. No deviations have been observed to date. Figure 1 shows a comparison of some of those measurements (note the logarithmic scale). The most precise CPT test for leptons stems from the comparison of the g factors of the electron and the positron to 2×10^{-9} [6]. The best verification for baryons and antibaryons is from the proton–antiproton charge-to-mass ratio measured in a Penning trap [7]. Finally, the mass difference of the neutral K meson and its antiparticle, with a relative uncertainty of only 3×10^{-19} , yields the best verification of CPT invariance for mesons (though this result is model-dependent) [8].

In the last two decades, immense progress has been made in the field of high-precision atomic spectroscopy of the hydrogen atom. The transition between the atomic ground ($1s$) and first excited ($2s$) state of hydrogen can be measured to 2 parts in 10^{14} [9]. For this purpose, a cold (7 K) hydrogen beam is brought into overlap in a resonant cavity with a laser beam whose wavelength is precisely double that of the $1s$ – $2s$ transition, thereby allowing (first-order) Doppler-free two-photon excitation. A quenching microwave field, which is turned on alternatingly with the exciting laser, resets the atoms from the metastable ($\tau = 122$ ms) $2s$ state to the short-lived ($\tau = 1.6$ ns) $2p$ state whose decay to the ground state by emission of a 121-nm photon is detected with a photomultiplier tube. This achievement paves the way for a CPT test with hydrogen and antihydrogen that could considerably improve the experimental limits for both leptons and baryons. It must be pointed out, however, that the actual

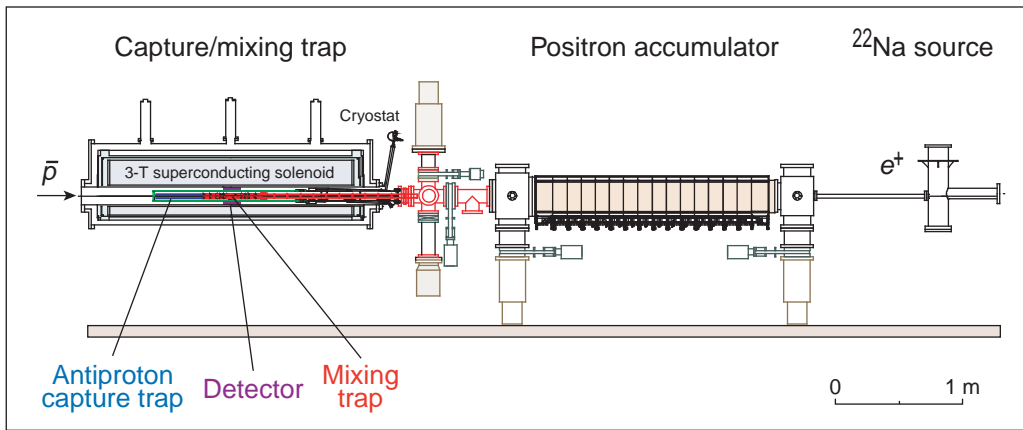


Figure 2: Overview of the ATHENA apparatus. Shown on the left is the superconducting 3-T solenoid magnet which houses the capture trap, the mixing trap, and the antihydrogen annihilation detector. On the right, the radioactive sodium source for the positron production and the 0.14-T positron accumulation Penning trap.

quantity measured in such a comparison is the ratio of the Rydberg constant to the anti-Rydberg constant. Since that ratio is a function of the charges and the masses of the proton and the electron as well as their antiparticles, possible CPT violating terms could cancel out.

The second domain of fundamental tests that could be carried out with antihydrogen concerns antimatter gravity. The Equivalence Principle of General Relativity, in particular the universality of free fall, has been well tested with ordinary matter [10]. Examples for instruments used in these tests are torsion balances [11] and atomic fountains [12]. On the other hand, no macroscopic bodies of antimatter are available, and precision tests with charged elementary anti-particles are hampered by the relative strength of the electromagnetic force with respect to gravity. This difficulty could be overcome with neutral antimatter atoms, under the condition that confinement and cooling of anti-atoms in a neutral-particle trap can be achieved. Possible deviations from the Weak Equivalence Principle could arise from gravitational scalar or vector fields. These effects could very well be stronger than possible CPT violations, because the gravitational pull by ordinary matter on antimatter does not constitute the CPT-symmetric situation to matter–matter attraction.

Any high-precision measurement of a ground state property requires a cold sample and long observation times. A large supply of the studied species is helpful and in some cases, such as for experiments using a beam of particles, absolutely required. It was therefore the declared goal of the ATHENA Collaboration (and also of its direct competitor ATRAP) to attempt to demonstrate the production of antihydrogen from cold antiprotons and positrons trapped in a charged-particle trap and to furthermore optimize the number of produced antihydrogen atoms and study their properties. These constitute the main objectives of the ATHENA experiment for its first phase, which started with the commissioning of the CERN Antiproton Decelerator in 1999 and which will end with its temporary shutdown at the end of 2004.

2 Experimental Setup

The layout of the ATHENA apparatus is based on an independent preparation of cold antiprotons and positrons and their subsequent mixing in a common trap region [13]. The main element of the experiment is a superconducting solenoid magnet which contains the capture and mixing traps, two parts of a long cylindrical Penning trap (diameter 25 mm, total length ≈ 1 m; see Fig. 2). The magnet is operated at a field magnitude of 3 T. A cryostat with a liquid-helium circuit independent from that of the magnet cools the trap to a temperature of about 15 K.

The antiprotons are produced in the target area of the Antiproton Decelerator (AD) [14], where a thick iridium target is bombarded with a 24-GeV/c pulse of about 10^{13} protons. The antiprotons are separated from the secondary products such as pions and muons and $1\text{--}3 \times 10^7$ \bar{p} are injected into the

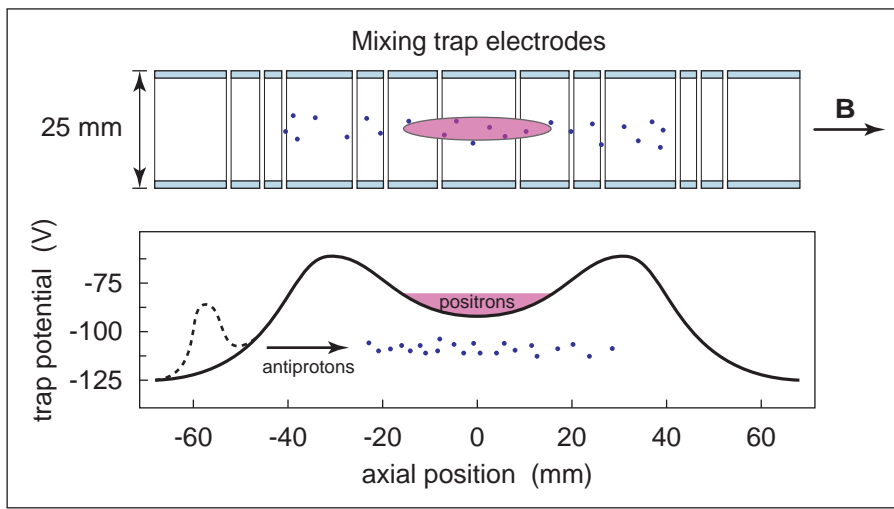


Figure 3: Detailed sketch of the mixing trap, which is operated in a nested-trap configuration [16]. The bottom graph shows the axial trap potential before (dashed line) and after (solid line) the antiproton injection.

AD at a momentum of ≈ 3.5 GeV/ c . This antiproton bunch is then decelerated in several stages and radially cooled by stochastic (velocity $v \approx c$) and electron cooling ($v \approx 0.3$ – $0.1c$). After about 100 s, the pulse is extracted at 100 MeV/ c (≈ 5 MeV kin. energy) and delivered to one of the experiments. ATHENA performs the last deceleration step from the AD final energy of about 5 MeV by letting the antiprotons pass through a thin (≈ 50 μm) degrader foil. The foil thickness is chosen so as to maximize the fraction of \bar{p} with an energy of less than 5 keV, thereby allowing an efficient stopping by electrostatic potentials. In the capture trap, the $\approx 10^4$ antiprotons per AD spill lose energy by collisions with a plasma of about 10^8 electrons which have been loaded into the trap and allowed to cool.

In parallel, positrons are produced from a strong source of radioactive ^{22}Na , which decays to ^{22}Ne by emitting highly energetic β radiation. The positrons are moderated in a layer of solid neon and cooled and accumulated in the axial potential minimum of a buffer-gas-filled 0.14-T Penning trap. After each accumulation cycle of about 200 s, between 5×10^7 and 1.5×10^8 positrons are available for transfer to the recombination region. There, the number, density, aspect ratio, and relative temperature of the positron plasma can be non-destructively measured with a detection system that resonantly excites and detects the first and second axial plasma modes [15].

The mixing of antiprotons and positrons takes place in a second cylindrical Penning trap in the superconducting solenoid. This so-called mixing trap is shown schematically in Fig. 3. In order to simultaneously trap particles of opposite charge, the axial electrostatic potential in the recombination region is operated in a so-called nested-trap configuration [16]. The central well is first filled with the positrons, which cool to the ambient temperature of 15 K with a time constant of about 0.5 s by synchrotron radiation due to their high cyclotron frequency in the strong magnetic field. The $\approx 10^4$ antiprotons are initially transferred to a small lateral well (dashed line in Fig. 3) and then launched into the nested-well region with a kinetic energy of about 30 eV. The antiprotons cool in collisions with the positrons and after about 20–30 ms $\bar{\text{H}}$ production sets in. Neutral antihydrogen atoms are no longer confined in the charged-particle trap and leave the interaction region with a momentum essentially equal to that of the antiproton just before recombination. They hit the trap electrodes, where their constituents annihilate with their ordinary-matter counterparts in quick succession. The mixing cycle currently lasts about 70 s and is repeated every 250 s.

The signal of the $\bar{\text{H}}$ annihilations is recorded with the ATHENA antihydrogen detector, positioned coaxially with the mixing trap within the magnet bore. It is a crucial component of this experiment and sets it apart from its competitor. The active components of the ATHENA detector are shown schematically in Fig. 4. It consists of a highly granular array of 8192 silicon strips in two layers and 192 CsI crystals read out by avalanche photo diodes, all within a radial extent of only 140 mm. The Si detectors record the signal of the charged pions produced in the \bar{p} - p annihilation; three or more

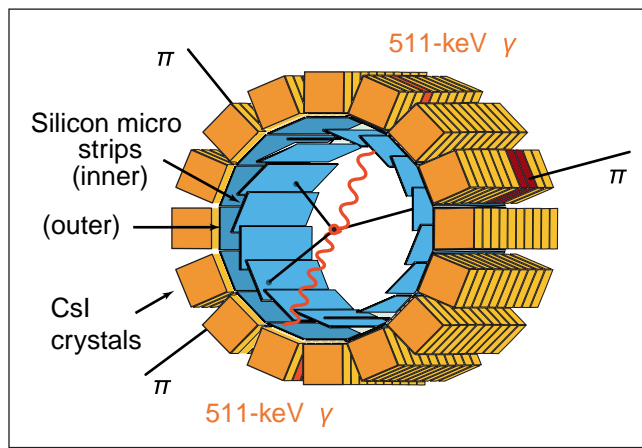


Figure 4: Sketch of the ATHENA antihydrogen annihilation detector. With its highly granular silicon strip and CsI crystal modules, it allows a direct and unambiguous detection of $\bar{\text{H}}$ production.

hits in the outer Si layer trigger a readout of the complete detector. Depending on the multiplicity of the charged decay products, the Si detector hits can in most cases be used to reconstruct the vertex of the annihilation. The resolution of this reconstruction, about 4 mm, is limited by the fact that the curvature of the charged-particle tracks cannot be reconstructed from only two detector hits per track. The array of crystals detects the photons from the e^+e^- annihilation, most of which ($> 95\%$) have a multiplicity of two and are hence emitted back-to-back, *i.e.* with an opening angle of 180° as seen from the reconstructed vertices from the charged particles.

Figure 5 shows the signal obtained with this detector in a number of mixing cycles, as published in ATHENA’s report on the first production of cold antihydrogen in September 2002 [17]. The top panels show the number of recorded events from the silicon detector as a function of the azimuthal coordinates. The highest number of events, shown in red, is recorded at the trap electrodes at $r = 12.5$ mm as expected for antihydrogen annihilation. When the positron plasma is heated to several 1000 K by an RF excitation of its axial plasma modes, the $\bar{\text{H}}$ production is suppressed and only a much lower number of events, from antiproton annihilations with trapped residual gas ions or neutral contaminants, is detected (top right panel). The lower panels of Fig. 5 show the number of 511-keV γ events recorded in the crystal detector as a function of the opening angle $\theta_{\gamma\gamma}$. For cold positrons, the data shows a clear peak for an opening angle of 180° which disappears when the positrons are heated. The right panel illustrates the excellent agreement with a Monte Carlo simulation. In Ref. 17, it was deduced from Monte Carlo simulations that the 131 fully reconstructed events that constitute the peak in the lower left panel of Fig. 5 corresponded to a total number of about 50 000 produced $\bar{\text{H}}$ atoms.

In the months after ATHENA’s initial report, the ATRAP Collaboration also reported the production of cold antihydrogen [18]. Due to the lack of a position-sensitive $\bar{\text{H}}$ annihilation detector, ATRAP adopted an indirect detection scheme in which antihydrogen that is emitted along the trap axis is re-ionized in a strong electric field and the resulting antiprotons are captured in an axial potential well. This allows a practically background-free observation at the expense of a very small solid angle for detection.

A more complete analysis of our data from 2002, together with more detailed Monte Carlo simulations, showed that the instantaneous trigger rate from the silicon detector is a good proxy for antihydrogen production, with 65% of all triggers over the entire mixing cycle due to annihilating antihydrogen atoms [19]. A total of about 2×10^6 antihydrogen atoms were produced by ATHENA in 2002 and 2003 combined.

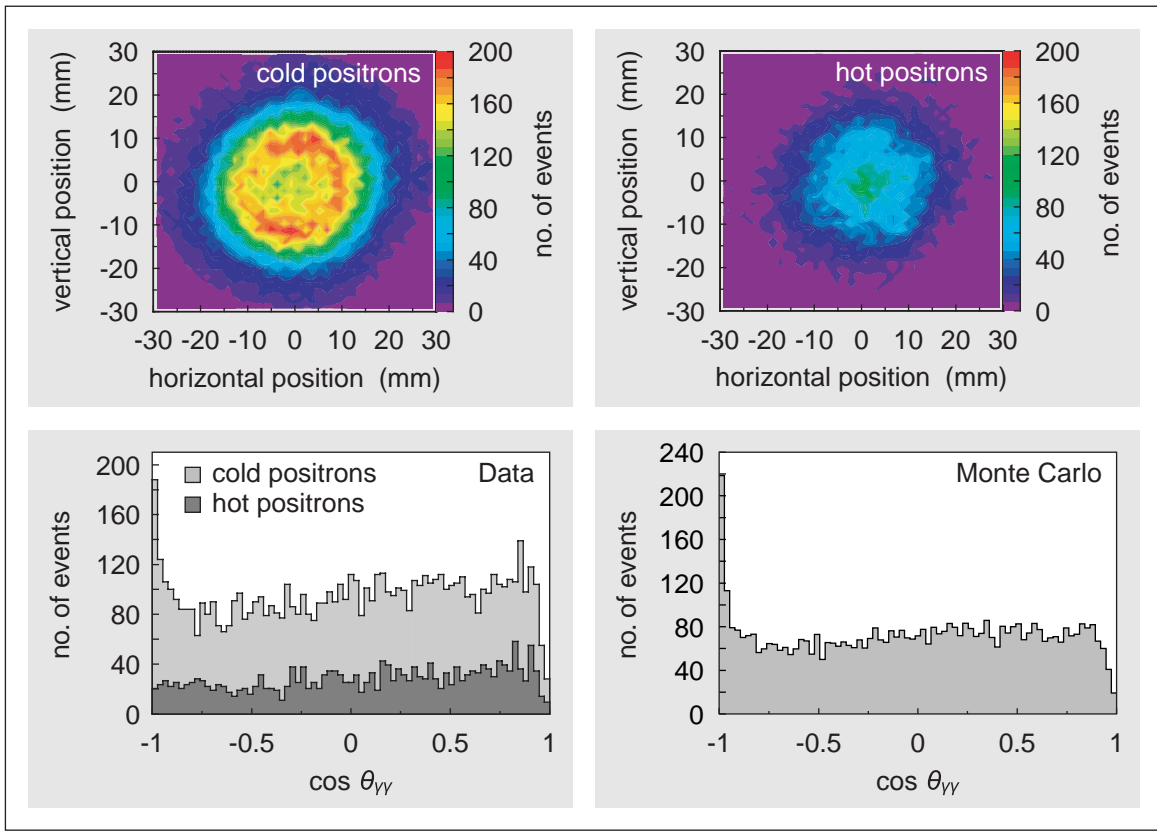


Figure 5: Signal for the first production of cold antihydrogen with ATHENA [17]. (top) Charged-pion vertex distribution as a function of the azimuthal coordinates; (bottom) Opening-angle distribution of the photons recorded in coincidence with the charged-particle hits.

3 Recent Studies

3.1 Antiproton cooling

As mentioned previously, the positron plasma confined in the 3-T Penning trap cools rapidly ($\tau \approx 0.5$ s) to the temperature of the surrounding electrodes by synchrotron radiation. The cooling of the antiprotons in this cold e^+ plasma is a much more complicated process because it is caused by Coulomb interactions with the positron plasma and because of the unknown radial extent of the \bar{p} cloud. We have conducted a series of experiments to study this cooling process, in which the nested wells of the mixing trap were slowly emptied at varying times after the \bar{p} injection, allowing a measurement of the \bar{p} energy distribution at that time [20]. The result of these measurements is shown in Fig. 6 (only the dump of the left lateral antiproton well is shown). The figure shows the presence of two distinct cooling processes with very different time constants. A large portion of the antiprotons rapidly attains thermal equilibrium with the positrons (Region II) with a time constant of $\tau \approx 10$ ms. This time corresponds to the observed onset of high-rate production of antihydrogen. On a much longer time scale of about 50 s, another large fraction of the injected \bar{p} cools into Region II. The first is attributed to antiprotons which initially overlap with the positrons and which are cooled very efficiently in Coulomb collisions. The second cooling phase is probably due to antiprotons which have a larger initial radius and interact only with a thin tail of the positron plasma or possibly with residual-gas ions surrounding it. A population of Region III, below the positron energy, is also observed. This is probably due to $\bar{p}-\bar{p}$ collisions in the lateral wells that transfer longitudinal to radial momentum or re-ionized Rydberg \bar{H} atoms. In the absence of positrons, no cooling takes place and the \bar{p} cloud still has the initial kinetic energy even after 190 s.

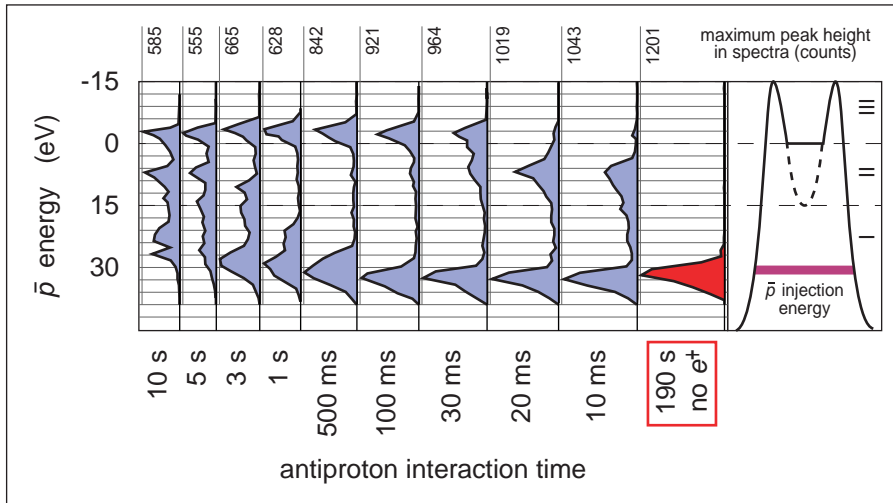


Figure 6: Energy distribution of antiprotons, dumped from the nested trap at varying times after injection [20].

Table 1: Comparison of some of the properties of three-body recombination and spontaneous radiative recombination, believed to be the dominant processes for antihydrogen production at ATHENA. The SRR rate was calculated for $T = 15$ K, $n_{e^+} = 2 \times 10^8/\text{cm}^3$, and $N_{\bar{p}} = 10^4$ [23].

	Three-body recombination	Spont. radiative recombination
Temperature dep.	$\propto T^{-9/2}$	$\propto T^{-0.63}$
Positron density dep.	$\propto n_{e^+}^2$	$\propto n_{e^+}$
Cross-section at 1 K	10^{-7} cm^2	10^{-16} cm^2
Final internal states	$n \gg 10$	$n < 10$
Expected rates	unknown	$\approx 40 \text{ Hz}$

3.2 Recombination process

The process that leads to the recombination of antiprotons and positrons for the formation of antihydrogen is of the utmost importance. It has crucial implications both for the optimization of antihydrogen production and for the internal (atomic) states of the produced anti-atoms. The capture of a positron by an antiproton into a bound atomic state cannot simultaneously conserve energy and momentum; the excess momentum has to be carried away by a third reaction partner. The dominant processes for $\bar{\text{H}}$ production are believed to be three-body recombination (TBR) and spontaneous radiative recombination (SRR), in which this third particle is a second positron or a photon, respectively [21, 22]. These two processes exhibit some very different properties, summarized in Tab. 1. Since high-precision measurements have to be carried out on anti-atoms in the ground state, the most important difference between the production mechanisms is in the final atomic states that they populate. While SRR creates final states with low principal quantum numbers, TBR produces Rydberg atoms with $n \gg 10$. These excited states are expected to decay very rapidly to the ground state, but they can also easily be re-ionized in the strong electric fields present in the mixing region. Under real experimental conditions, an equilibrium between de-excitation and re-ionization will probably set in.

As is also shown in the table, the rates of the two recombination mechanisms follow different power laws as a function of temperature and positron density. We have recently studied the temperature dependence of the recombination rate in order to determine the dominant recombination process under the experimental conditions of ATHENA [23]. We performed antiproton–positron mixing under otherwise standard conditions, but varying the positron temperature by RF heating of the axial plasma modes. From these data we extracted the opening angle excess, the total number of triggers in a complete mixing cycle (background-corrected), and the peak trigger rate as possible proxies for the instantaneous recombination rate. The latter two are shown in Fig. 7. All of these variables show a very

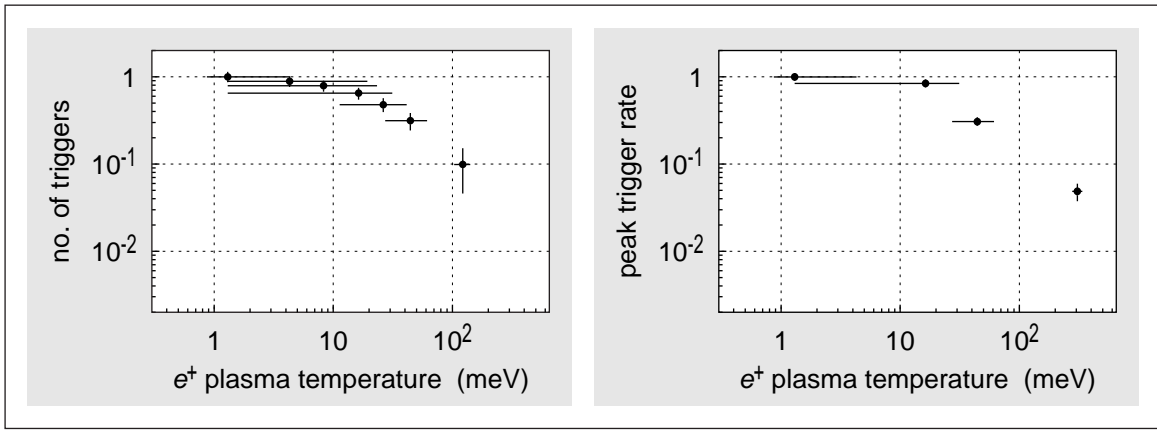


Figure 7: Dependence of the background-corrected integrated total number of charged-particle triggers per mixing cycle (left) and the peak trigger rate (left) on the positron plasma temperature [23]. Note the logarithmic scale.

similar temperature dependence: The production decreases strongly with increasing temperature (as expected from the power laws given in Tab. 1), but there is also a turnover for the lowest temperatures and the overall shape of the graphs does not correspond to the straight line expected for a simple power law (note the logarithmic scale). More detailed calculations of the recombination rates, taking into account the magnetic and electrostatic fields in the recombination region, may eventually explain this intriguing behavior. A fit with a power law of the form T^α to the peak trigger rate data yields $\alpha = -0.7(2)$, in close agreement with that expected for spontaneous radiative recombination.

4 Conclusions and Outlook

ATHENA can routinely produce several hundred cold antihydrogen atoms per minute. These numbers allow detailed studies of the properties of the produced $\bar{\text{H}}$, such as the process responsible for antihydrogen recombination. The temperature dependence of the antihydrogen production rate has been studied quantitatively. A best fit to the data suggests spontaneous radiative recombination as the dominant formation process, even though the observed rates are at least an order of magnitude larger than predicted. An ongoing analysis of the 2003 data with respect to the positron density dependence should shed more light on this important question. Notwithstanding the already large antihydrogen production efficiency (with respect to captured antiprotons from the AD) of about 15%, a more complete understanding of the recombination process and a further increase of its efficiency are important. For this purpose, efforts are underway to enhance $\bar{\text{H}}$ production by laser-stimulated recombination. This will also constitute a first spectroscopic measurement on antihydrogen. Furthermore, it is planned to employ a radiofrequency excitation of the antiprotons' characteristic motions in the Penning trap in order to center them and enhance the transfer efficiency from the capture trap to the mixing trap and to improve the radial overlap between the antiprotons with the positron plasma.

Acknowledgments

This work was supported by the funding agencies INFN (Italy), CNPq (Brazil), MEXT (Japan), SNF (Switzerland), SNF (Denmark), and EPSRC (United Kingdom).

References

- [1] C. S. Wu *et al.*, Phys. Rev. **105** (1957) 1413.
- [2] J. H. Christenson *et al.*, Phys. Rev. Lett. **13** (1964) 138.
- [3] W. Pauli, Il Nuovo Cimento **6** (1957) 6.
- [4] J. R. Ellis *et al.*, Phys. Lett. B **293** (1992) 142.

- [5] R. Bluhm *et al.*, Phys. Rev. D **57** (1998) 3932.
- [6] R. S. Van Dyck *et al.*, Phys. Rev. Lett. **59** (1987) 26.
- [7] G. Gabrielse *et al.*, Phys. Rev. Lett. **82** (1999) 3198.
- [8] H. B. Hsiung *et al.*, Nucl. Phys. B (PS) **86** (2000) 312.
- [9] M. Niering *et al.*, Phys. Rev. Lett **84** (2000) 5496.
- [10] E. G. Adelberger, B. R. Heckel, and A. E. Nelson, Annu. Rev. Nucl. Part. Sc. **53** (2003) 77.
- [11] B. R. Heckel *et al.*, Adv. Space Res. **25** (2000) 1225.
- [12] A. Peters *et al.*, Nature **400** (1999) 849.
- [13] M. Amoretti *et al.*, Nucl. Instrum. Methods A **518** (2004) 679.
- [14] J. Y. Hémery and S. Maury, Nucl. Phys. A **655** (1999) 345c.
- [15] M. Amoretti *et al.*, Phys. Rev. Lett. **91** (2003) 055001.
- [16] G. Gabrielse *et al.*, Phys. Lett. A **129** (1988) 38.
- [17] M. Amoretti *et al.*, Nature **419** (2002) 456.
- [18] G. Gabrielse *et al.*, Phys. Rev. Lett. **89** (2002) 213401.
- [19] M. Amoretti *et al.*, Phys. Lett. B **578** (2004) 23.
- [20] M. Amoretti *et al.*, Phys. Lett. B **590** (2004) 133.
- [21] M. E. Glinsky *et al.*, Phys. Fluids B **3** (1991) 1279.
- [22] J. Stevedfelt *et al.*, Phys. Rev. A **12** (1975) 1246.
- [23] M. Amoretti *et al.*, Phys. Lett. B **583** (2004) 59.